Broadband Terahertz Power Detectors Based on 90-nm Silicon CMOS Transistors With Flat Responsivity Up to 2.2 THz

Kęstutis Ikamas, *Student Member, IEEE*, Dovilė Čibiraitė, Alvydas Lisauskas, *Member, IEEE*, Maris Bauer, Viktor Krozer, *Senior Member, IEEE*, and Hartmut G. Roskos

***Abstract*— We present broadband high sensitivity terahertz (THz) detectors based on 90 nm CMOS technology with the state-of-the-art performance. The devices are based on bow-tie and log-spiral antenna-coupled field-effect transistors (FETs) for the detection of free-space THz radiation (TeraFETs). We report on optimized performance, which was achieved by employing an in-house developed physics-based model during detector design and thorough device characterization under THz illumination. The implemented detector with bow-tie antenna design exhibits a nearly flat frequency response characteristic up to 2.2 THz with an optical responsivity of 45 mA/W (or 220 V/W). We have determined a minimum optical noise-equivalent power as low as 48 pW/$\sqrt{\text{Hz}}$ at 0.6 THz and 70 pW/$\sqrt{\text{Hz}}$ at 1.5 THz. The results obtained at 1.5 THz are better than the best narrowband TeraFETs reported in the literature at this frequency and only up to a factor of four inferior to the best narrowband devices at 0.6 THz.**

***Index Terms*— THz power detector, terahertz detector, submillimeter-wave detector, broadband antenna, field-effect transistor, FET device modeling, rectification.**

I. Introduction

DETECTION of THz radiation (0.3-10 THz) remains a formidable task for high sensitivity direct receivers of THz power. THz radiation is generated by a variety of radiation sources such as optoelectronic emitters (photoconductive mixers, nonlinear optical crystals), electronic emitters usually including multiplier chains, semiconductor lasers such as quantum cascade lasers, molecular gas lasers, vacuum electronic devices, gyrotrons, etc. The THz power generated by these sources can be detected using room-temperature operated rectifying devices such as Schottky and tunneling diodes [1], [2] and FETs [3]. These devices can be implemented as direct power detectors or in homodyne or heterodyne coherent detection mode. In addition, THz detector arrays can be utilized for imaging purposes. One advantage of TeraFETs as THz power detectors is that they can be fabricated using mainstream semiconductor device technologies and hence can be realized as large area arrays.

A limitation of such detectors often is their restricted bandwidth. This is not owed to an intrinsic shortcoming of the rectification process itself but rather induced by external components such as waveguides or antennas. Monolithic integration of antennas and TeraFET detector devices allows one to minimize reactive elements and to achieve broadband operation with competitive noise-equivalent power (NEP) performance. In this letter, we demonstrate a THz detector with a flat responsivity over a frequency range spanning more than three octaves (from 0.25 to 2.2 THz).

II. TeraFET Design

TeraFET detectors were fabricated using a 90-nm silicon CMOS process (TSMC). We used transistors with a channel length of 100 nm and a width of 1 μm. Two broadband antenna designs were implemented, namely a bow-tie and a log-spiral version, see the left side of Fig. 1. In order to optimize THz power coupling, a single-transistor layout was chosen in contrast to our previous double-FET designs [4]–[6].

The right side of Fig. 1 illustrates the basic layout of the detector. The THz radiation is coupled in from the bottom through the substrate and received by the antenna which is integrated into the metal/insulator stack of the CMOS backend. Each antenna leaf is formed by segments patterned into two metal sheets - the thick top metal and that of the eighth metal layer. The metal sheets of the source-side antenna leaf are connected with each other. On the drain side, only the top metal connects directly to the drain electrode whereas the eighth-layer metal is connected with the gate electrode which allows for both independent DC-biasing of the gate and readout of the rectified signal through the source and drain contacts. The gate and drain leafs are capacitively coupled, hence on the same THz potential, which ensures asymmetric power coupling into the channel from the source side only, an essential condition for efficient plasma-wave rectification [5], [7], [8]. Inclusion of the ninth metal layer serves for

Manuscript received June 29, 2018; revised July 18, 2018; accepted July 21, 2018. Date of publication July 24, 2018; date of current version August 23, 2018. This work was supported by the Research Council of Lithuania under Contract TAP LZ-06/2015, in part by the Hessian excellence initiative LOEWE–Terahertz-Kamera für die zivile Sicherheitstechnik, in part by the EU Horizon 2020 Marie Sklodowska-Curie ITN CELTA project under Grant 675683, and in part by ESA through the THzFET Project. The review of this letter was arranged by Editor L. K. Nanver. *(Corresponding author: Kęstutis Ikamas.)*

K. Ikamas is with the Faculty of Physics, Vilnius University, LT-10257 Vilnius, Lithuania, and also with the Military Academy of Lithuania, LT-10322 Vilnius, Lithuania (e-mail: kestutis.ikamas@ff.vu.lt).

D. Čibiraitė and H. G. Roskos are with the Physikalisches Institut, Goethe-Universität, D-60438 Frankfurt, Germany.

A. Lisauskas is with the Faculty of Physics, Vilnius University, LT-10257 Vilnius, Lithuania.

M. Bauer is with the Center for Materials Characterization and Testing, Fraunhofer ITWM, D-67663 Kaiserslautern, Germany, and also with the Physikalisches Institut, Goethe-Universität, D-60438 Frankfurt, Germany.

V. Krozer is with the Physikalisches Institut, Goethe-Universität, D-60438 Frankfurt, Germany, and also with the Ferdinand-Braun-Institut, Leibniz-Institut für Höchstfrequenztechnik, 12489 Berlin, Germany.

Color versions of one or more of the figures in this letter are available online at http://ieeexplore.ieee.org.

Digital Object Identifier 10.1109/LED.2018.2859300

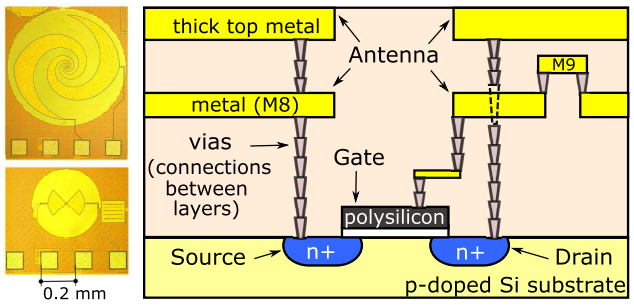

Fig. 1. Left: Micrographs of TeraFETs with log-spiral (top) and bow-tie antenna (bottom). The bow-tie antenna has an opening angle of 90°, the length of each leaf is 105 μm. Right: A simplified cross-sectional view of the transistor region of the TeraFET. Elements in the view are not to scale.

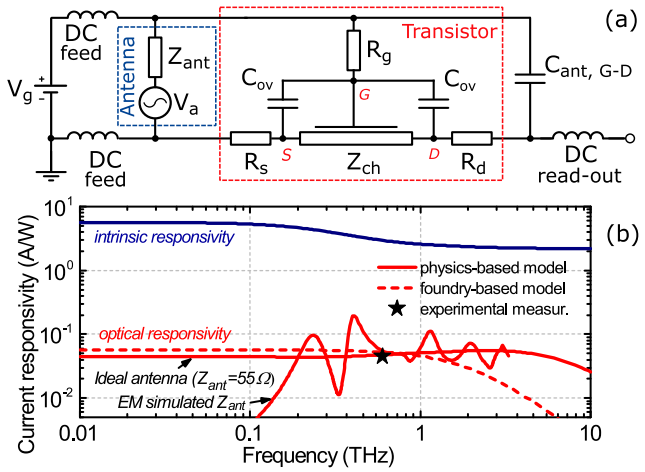

Fig. 2. (a) A simplified equivalent circuit of the TeraFET. (b) Simulated and measured current responsivity vs. radiation frequency for the TeraFET at V_g=0.45 V. The optical $\Re_I$ was simulated separately with the foundry-based (dashed line) and the physics-based models (red solid lines). The intrinsic responsivity was simulated only with the latter model (dark blue line). The responsivity of the TeraFET with a bow-tie antenna measured at 600 GHz is denoted by a black star.

protection of the FET against electrostatic discharge due to charge accumulation on the gate electrode during eighth-layer patterning. In order to reduce loss in p-doped Si substrate it was thinned to 280 μm.

III. Device Model

The high-frequency modeling of the detector was performed using (i) the standard transistor model provided by the foundry TSMC and implemented in the Keysight ADS software environment and (ii) an analytic model with a kernel describing the rectification process in the FET with the help of a distributed transmission line description channel model. We discuss this model which – unlike the one provided by the foundry – enables us to take charge-density waves in the channel into account. The transistor and its environment including the antenna are presented in the form of an equivalent circuit shown in Fig. 2(a).

For the calculation of the current responsivity $\Re_I$ to small-signal THz excitation, we start with the Dyakonov-Shur hydrodynamic model of transport in the channel [8]. The rectification process can be represented either as an equivalent current source (as in [5]) or an equivalent voltage source. Following the latter approach here, we derive the current responsivity from the small-signal voltage response ΔV to excitation with unity THz voltage amplitude directly at the entrance to the gated part of the channel, multiplied by the factor $\eta H_V^2 8\mathrm{Re}(Z_{ant})P_0$. Here, η takes into account both optical coupling losses and the antenna efficiency, Z_{ant} is the antenna impedance, and H_V accounts for the voltage attenuation upon signal transfer from the antenna to the transistor's channel. The product $8\mathrm{Re}(Z_{ant})P_0$ refers to the amplitude squared of the equivalent voltage source V_a with P_0 representing maximum available power (the beam power) [9, p. 78]. With the prediction of the hydrodynamic model for ΔV, one obtains:

$$\Re_I = \frac{\Delta V}{P_0 \cdot R_{DC}} = \frac{q f(\omega,\tau)}{4 s^2 m^*} \cdot \frac{\eta H_V^2 8\mathrm{Re}(Z_{ant})}{R_{DC}} \qquad (1)$$

with $m^* = 0.26 \cdot m_e$ being the effective mass of electrons in Si (m_e - the free electron mass) and τ the momentum scattering time, q the elementary charge, ω the angular frequency of the THz wave, and $f(\omega,\tau)$ the efficiency factor introduced in [8]. R_{DC} is the quasi-static drain-source resistance. The plasma velocity s depends on the carrier density n in the gated part of the transistor channel and its modulation by the gate voltage V_g according to $s = \sqrt{(q/m^*)\, n \partial V_g/\partial n}$. As n is inversely proportional to the DC resistance R_{ch} of the gated part of the channel, the quantity $n\partial V_g/\partial n$ can be expressed by $\left|R_{ch}\partial V_g/\partial R_{ch}\right|$, which permits one to quantify it based on measurements of R_{DC}. For the frequency-dependent conversion efficiency factor f, we use the expression: $f(\omega,\tau) = 1 + 2\omega\tau/\sqrt{1+(\omega\tau)^2}$. It holds for the condition of non-resonant plasma waves $s\tau/L \ll 1$ (L being the gate length) [4], and ac-shorted drain and gate.

The impedance of the antenna and parasitic device elements shown if Fig. 2(a) define the voltage attenuation factor H_V. In the strong inversion regime, these parasitic elements can directly influence the detection mechanism itself [10]–[12]. Here, we take into account three parasitic elements: the contact resistance R_s, the shunting capacitance Z_{par} (subsuming fringe and overlap capacitances), and the gate resistance R_g:

$$H_V = \left| \frac{Z_{ch} || Z_{par}}{Z_{ch} || Z_{par} + R_s + R_g + Z_{ant}} \right|, \qquad (2)$$

where $Z_{ch} = -ik\tau s^2 \tanh(kL) R_{ch}/(\omega L)$ is the impedance of the gated FET channel and $k = \omega/s \cdot \sqrt{1 - i/(\omega\tau)}$ is the wave number. Here we assume that $Z_{par} = 1/(i\omega C_{ov})$ is determined by the overlap capacitance $C_{ov} \approx 0.072$ fF, located between the source and gate terminals, which is in close agreement with Suzuki's model [13].

For the evaluation of Eq. 1, we need to determine the scattering time τ (or the electron mobility μ), R_s, η, and Z_{ant}. The first two parameters are derived by fitting the measured R_{DC} using the procedure described in [14]. Assuming equal source and drain contact resistances we estimate $2 \cdot R_s = 151\ \Omega$ and $\mu = 358\ \mathrm{cm^2/(V \cdot s)}$ yielding $\tau = 52.8$ fs. With this value we obtain $s\tau/L \approx 0.13$ in the vicinity of $V_{th} = 0.48$ V, supporting the non-resonant-plasmon approximation. The obtained carrier mobility is in a good agreement with values which are commonly cited in the literature as typical for Si of comparable doping [15].

Fig. 2(b) displays the simulated intrinsic and optical current responsivities as a function of frequency for a gate voltage of $V_g = 0.45\,V$ where the detector exhibits best NEP. The factor η is assumed to be 0.2 (having antenna

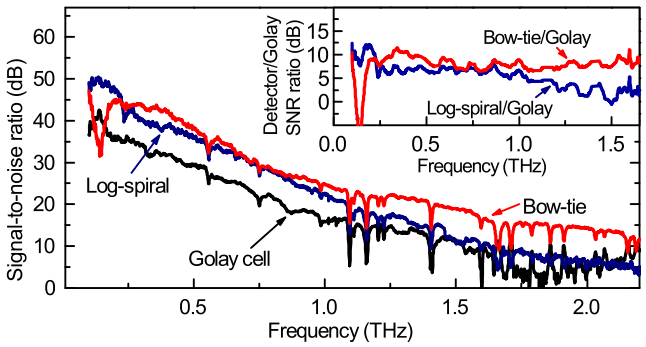

Fig. 3. Comparison of the frequency-dependent SNR of the THz detectors ($V_g = 0.45$ V) and a commercial Golay cell. Inset: The SNR ratios of the TeraFET and the Golay cell detectors.

efficiency ≈ 0.4, transmission at the Si surface ≈ 0.7, and Gaussian beam coupling efficiency ≈ 0.7), and the frequency-independent antenna impedance of $Z_{ant} = 55\ \Omega$ is estimated for self-complementary antennas on Si employing Babinet's principle [16, p. 697]. In addition, we show a prediction for electromagnetically (EM) simulated frequency-dependent impedance Z_{ant} of the bow-tie antenna shown in Fig. 1. The intrinsic responsivity is calculated using Eq. 1 by replacing the P_0 by the power directly absorbed in Z_{ch} [9, p. 77]. In this case the term $\eta H_V^2 8\mathrm{Re}(Z_{ant})/R_{DC}$ is substituted by $(2\mathrm{Re}(1/Z_{ch})R_{ch})^{-1}$.

The model predicts a fairly flat intrinsic responsivity of several A/W with a moderate decline of the rectified signal starting from 0.1 THz. The simulated optical responsivity is two orders of magnitude lower, but also exhibits a flat frequency response. For frequencies below 1 THz, the responsivity calculated with the physics-based model (solid line) and that based on the foundry model (dashed line) are in a good agreement with each other. The difference between the two models is within a 25% margin. However, above 1 THz the physics-based model predicts a slight rise of responsivity instead of a clear roll-off as found with the foundry-based model (the difference is in the order of $\sim 3.9\times$ at 2.8 THz).

IV. Broadband THz Characterization

We characterized TeraFETs from 0.1 up to 2.2 THz using a photomixer-based THz source (TOPTICA TeraScan 1550 [17]) and compared signal-to-noise ratios (SNR) of our TeraFETs with a Golay cell. The source provides a maximum THz output power of 40 μW at 0.1 THz decreasing exponentially with frequency. Due to sensitivity limitations of calibrated power meter, we determined absolute responsivity values using an all-electronic VDI source with 66 μW output power at 0.6 THz where the TeraFETs show best performance. A silicon substrate lens in aplanatic optical configuration [18] couples the radiation onto the detectors in both setups.

For our bow-tie TeraFET we find a responsivity of 45 mA/W at 0.6 THz, which is in very good agreement with the prediction of the simulations (see Fig. 2(b)). The minimum optical NEP (i.e., referenced to the available beam power) was 48 pW/$\sqrt{\mathrm{Hz}}$, a value which is only a factor of 2-4 higher than that of the best narrow-band TeraFETs made in Si CMOS [19] and is on a par with the best broadband AlGaN/GaN TeraFETs [14]. The log-spiral-coupled TeraFET showed a slightly higher NEP with 100 pW$\sqrt{\mathrm{Hz}}$ and a responsivity of 11 mA/W (not accounting for a polarization loss).

We present in Fig. 3 the frequency-dependent signal-to-noise ratios (SNRs) of our TeraFETs and compare them with the SNR of a commercial Golay cell (Tydex). The measurements were performed with a lock-in amplifier at the modulation frequency of 888 Hz and 20 Hz, and the time constant of 500 ms and 2 s for TeraFETs and Golay cell, respectively. A higher value of the modulation frequency was chosen for the TeraFET to save the experiment time as it does not affect detector's responsivity. Since the channel of TeraFETs is unbiased, the output noise is limited only by thermal noise [20], [21].

The inset of Fig. 3 presents the ratios between SNRs of the TeraFET detectors and the Golay cell. The two curves show similar spectral modulations, which we attribute to etalon resonances in the diamond window of the Golay cell. Otherwise, the Golay cell can be assumed to exhibit a flat frequency response, although in these measurements, the low power levels above 1.75 THz lead to spurious peaks in the response due to water vapor in the cell – this spectral range was therefore omitted in the analysis. We find that the bow-tie TeraFET exceeds the dynamic range of the Golay cell by roughly 8 dB. The performance of the log-spiral TeraFET lies between the two devices. We conclude that the responsivity spectrum of the bow-tie TeraFET is also nearly flat. Given the minimum optical NEP of 48 pW/$\sqrt{\mathrm{Hz}}$ determined at 0.6 THz, one estimates an optical NEP of 70 pW/$\sqrt{\mathrm{Hz}}$ at 1.5 THz. The log-spiral TeraFET shows a narrower region of flat frequency response. We estimate the NEP to be 100 pW/$\sqrt{\mathrm{Hz}}$ in the range of 0.6-1.0 THz. We note that the strong dip in the SNR of the bow-tie detector around 150 GHz results from an interaction of the antenna with the surrounding metal (see the micrograph in Fig. 1). This can be estimated by taking the radius of the equivalent circular slot antenna which is equal to 200 μm and the effective dielectric constant $\varepsilon_{\mathrm{eff}} \approx 2.6$. The corresponding wavelength and frequency are, respectively, $\sim$2.0 mm and 150 GHz. In the measured frequency range the log-spiral design does not exhibit this feature because of larger dimensions.

V. Conclusion

In summary, the TeraFET with a bow-tie antenna exhibits a nearly flat frequency response characteristic from 0.4 THz up to 2.2 THz with an optical responsivity of 45 mA/W (or 220 V/W) at 0.6 THz. We have determined a minimum optical NEP as low as 48 pW/$\sqrt{\mathrm{Hz}}$ at 0.6 THz and 70 pW/$\sqrt{\mathrm{Hz}}$ at 1.5 THz. The results obtained at 1.5 THz are better than the best ones reported in the literature for narrowband TeraFETs at this frequency and only up to a factor of four inferior to the results of the best narrowband devices at 0.6 THz. The log-spiral design exhibits narrower range of flat responsivity, however has higher sensitivity below 230 GHz. Furthermore, a log-spiral antenna is more suited for measurements when the polarization of a THz beam is unknown or changes in time. We conclude that characterization results of a bow-tie coupled device above 1 THz are in better agreement with the analytical model rather than with the foundry-based model predictions. Our proposed device model correctly describes the performance of the detector as it predicts the THz detection well beyond 2 THz confirmed by measurements. We are not aware of any other physical approach which could provide results of similar accuracy.

REFERENCES

[1] G. C. Trichopoulos, H. L. Mosbacker, D. Burdette, and K. Sertel, "A broadband focal plane array camera for real-time THz imaging applications," *IEEE Trans. Antennas Propag.*, vol. 61, no. 4, pp. 1733–1740, Jan. 2013, doi: 10.1109/TAP.2013.2242829.

[2] M. Yahyapour, N. Vieweg, A. Roggenbuck, F. Rettich, O. Cojocari, and A. Deninger, "A flexible phase-insensitive system for broadband CW-terahertz spectroscopy and imaging," *IEEE Trans. THz Sci. Technol.*, vol. 6, no. 5, pp. 670–673, Sep. 2016, doi: 10.1109/TTHZ.2016.2589540.

[3] M. Bauer, R. Venckevičius, I. Kašalynas, S. Boppel, M. Mundt, L. Minkevičius, A. Lisauskas, G. Valušis, V. Krozer, and H. G. Roskos, "Antenna-coupled field-effect transistors for multi-spectral terahertz imaging up to 4.25 THz," *Opt. Express*, vol. 22, no. 16, pp. 19235–19241, Aug. 2014, doi: 10.1364/OE.22.019235.

[4] A. Lisauskas, U. Pfeiffer, E. Öjefors, P. H. Bolìvar, D. Glaab, and H. G. Roskos, "Rational design of high-responsivity detectors of terahertz radiation based on distributed self-mixing in silicon field-effect transistors," *J. Appl. Phys.*, vol. 105, no. 11, p. 114511, Jun. 2009, doi: 10.1063/1.3140611.

[5] S. Boppel, A. Lisauskas, M. Mundt, D. Seliuta, L. Minkevičius, I. Kašalynas, G. Valušis, M. Mittendorff, S. Winnerl, V. Krozer, and H. G. Roskos, "CMOS integrated antenna-coupled field-effect transistors for the detection of radiation from 0.2 to 4.3 THz," *IEEE Trans. Microw. Theory Techn.*, vol. 60, no. 12, pp. 3834–3843, Dec. 2012, doi: 10.1109/TMTT.2012.2221732.

[6] A. Lisauskas, S. Boppel, M. Mundt, V. Krozer, and H. G. Roskos, "Subharmonic mixing with field-effect transistors: Theory and experiment at 639 GHz high above f_T," *IEEE Sensors J.*, vol. 13, no. 1, pp. 124–132, Jan. 2013, doi: 10.1109/JSEN.2012.2223668.

[7] W. Knap, M. Dyakonov, D. Coquillat, F. Teppe, N. Dyakonova, J. Lusakowski, K. Karpierz, M. Sakowicz, G. Valušis, and D. Seliuta, "Field effect transistors for terahertz detection: Physics and first imaging applications," *J. Infr., Millim., Terahertz Waves*, vol. 30, no. 12, pp. 1319–1337, 2009, doi: 10.1007/s10762-009-9564-9.

[8] M. Dyakonov and M. Shur, "Detection, mixing, and frequency multiplication of terahertz radiation by two-dimensional electronic fluid," *IEEE Trans. Electron Devices*, vol. 43, no. 3, pp. 380–387, Mar. 1996, doi: 10.1109/16.485650.

[9] D. M. Pozar, *Microwave Engineering*, 4th ed. Hoboken, NJ, USA: Wiley, 2012.

[10] A. Lisauskas, M. Bauer, A. Rämer, K. Ikamas, J. Matukas, S. Chevtchenko, W. Heinrich, V. Krozer, and H. G. Roskos, "Terahertz rectification by plasmons and hot carriers in gated 2D electron gases," in *Proc. 41st Int. Conf. Noise Fluctuations (ICNF)*, Jun. 2015, pp. 1–5, doi: 10.1109/ICNF.2015.7288628.

[11] M. Shur, "Plasma wave terahertz electronics," *Electron. Lett.*, vol. 46, no. 26, pp. 18–21, Jan. 2010, doi: 10.1049/el.2010.8457.

[12] V. V. Popov, A. N. Koudymov, M. Shur, and O. V. Polischuk, "Tuning of ungated plasmons by a gate in the field-effect transistor with two-dimensional electron channel," *J. Appl. Phys.*, vol. 104, no. 2, p. 024508, Jul. 2008, doi: 10.1063/1.2955731.

[13] K. Suzuki, "Parasitic capacitance of submicrometer MOSFET's," *IEEE Trans. Electron Devices*, vol. 46, no. 9, pp. 1895–1900, Sep. 1999, doi: 10.1109/16.784191.

[14] M. Bauer, A. Rämer, S. Boppel, S. Chevtchenko, A. Lisauskas, W. Heinrich, V. Krozer, and H. G. Roskos, "High-sensitivity wideband THz detectors based on GaN HEMTs with integrated bow-tie antennas," in *Proc. 10th Eur. Microw. Integr. Circuits Conf. (EuMIC)*, Sep. 2015, pp. 1–4, doi: 10.1109/EuMIC.2015.7345053.

[15] S. Takagi, A. Toriumi, M. Iwase, and H. Tango, "On the universality of inversion layer mobility in Si MOSFET's: Part I—Effects of substrate impurity concentration," *IEEE Trans. Electron Devices*, vol. 41, no. 12, pp. 2357–2362, Dec. 1994, doi: 10.1109/16.337449.

[16] C. A. Balanis, *Antenna Theory: Analysis and Design*. Hoboken, NJ, USA: Wiley, Apr. 2005.

[17] A. J. Deninger, A. Roggenbuck, S. Schindler, and S. Preu, "2.75 THz tuning with a triple-DFB laser system at 1550 nm and InGaAs photomixers," *J. Infr., Millim., Terahertz Waves*, vol. 36, no. 3, pp. 269–277, 2015, doi: 10.1007/s10762-014-0125-5.

[18] J. van Rudd and D. M. Mittleman, "Influence of substrate-lens design in terahertz time-domain spectroscopy," *J. Opt. Soc. Amer. B, Opt. Phys.*, vol. 19, no. 2, pp. 319–329, Feb. 2002, doi: 10.1364/JOSAB.19.000319.

[19] G. Carpintero, L. E. García-Muñoz, H. L. Hartnagel, S. Preu, and A. V. Räisänen, Eds., *Semiconductor Terahertz Technology: Devices and Systems at Room Temperature Operation*. Hoboken, NJ, USA: Wiley, 2015.

[20] D. Čibiraitė, M. Bauer, A. Lisauskas, V. Krozer, H. G. Roskos, A. Rämer, V. Krozer, W. Heinrich, S. Pralgauskaitė, J. Zdanevičius, J. Matukas, A. Lisauskas, M. Andersson, and J. Stake, "Thermal noise-limited sensitivity of FET-based terahertz detectors," in *Proc. 41st Int. Conf. Noise Fluctuations (ICNF)*, Jun. 2017, pp. 320–323, doi: 10.1109/ICNF.2017.7986008.

[21] A. Lisauskas, S. Boppel, J. Matukas, V. M. Palenskis, L. Minkevičius, G. Valušis, P. Haring-Bolìvar, and H. G. Roskos, "Terahertz responsivity and low-frequency noise in biased silicon field-effect transistors," *Appl. Phys. Lett.*, vol. 102, no. 15, p. 153505, Apr. 2013, doi: 10.1063/1.4802208.